Novel transmitter designs for magnetic resonance imaging

Aussenhofer, S.A.

2

DESIGN AND EVALUATION OF A DETUNABLE WATER-BASED QUADRATURE HEM_{11} MODE DIELECTRIC RESONATOR AS A NEW TYPE OF VOLUME COIL FOR HIGH FIELD MRI

Sebastian A. AUSSENHOFER

Andrew G. WEBB

Parts of this chapter have been published in Magnetic resonance in medicine: official journal of the Society of Magnetic Resonance in Medicine **68**, 1325-31 (2012) [4].

2

An annular dielectric resonator made from distilled water has been designed to operate in degenerate quadrature HEM_{11} modes at 298.1 MHz (7 Tesla). The circularly polarized B_1^+ field has a high degree of homogeneity throughout a sample placed within the annulus. The sensitivity of the resonator was measured to be essentially identical to that of an eight-rung high-pass birdcage resonator with the same physical dimensions. High resolution in vivo images have been obtained from the human wrist. A new method of electronically detuning the resonator has also been evaluated. The design is extremely simple and rapid to build, with direct applicability to very high field imaging and also potential integration into human and animal hybrid position emission tomography (PET)/MRI and single-photon emission computed tomography (SPECT)/MRI systems due to the lack of conductor attenuation-induced artefacts in the reconstructed nuclear medicine images.

2.1. INTRODUCTION

DESIGNING radiofrequency (RF) coils for magnetic resonance (MR) becomes increasingly challenging at high values of the (operating frequency*coil diameter) product due to well-characterized increases in wavelength effects, radiation loss, and loss in capacitive lumped elements used for resonating and impedance matching the coil. Substitution of transmission line for lumped elements can mitigate some, but not all, of these effects ([14],[15]), with these transmission lines being used either in volume coils or as individual elements of a transmit array [11],[1]. In contrast to MR, electron paramagnetic resonance, which operates over a large frequency range from low GHz (X-band) to several hundreds of GHz (F- and D-band and above) primarily uses cavity resonator designs. Although some MR coil designs do have elements of resonant cavity behaviour, the emphasis for designing high field volume coils has so far been on adapting existing geometries from lower field strengths.

One promising candidate for a different type of high field MR coil is a dielectric resonator (DR) constructed from high permittivity material. DRs are used extensively in the communications and satellite industries. A large number of pure and mixed electromagnetic modes can be supported in a DR depending upon the geometry of the resonator. Computed modal structures of the spatial distribution of the magnetic and electric fields of cylindrical DRs have been shown by Kajfez et al. [8]. Visualization using MRI of many modes of a cylindrical DR has recently been demonstrated [16]. The two lowest frequency modes, the $TE_{10\delta}$ and $HEM_{11\delta}$ are shown in Figure 2.1, with the abbreviations representing transverse electric (TE) and hybrid electromagnetic (HEM), respectively. Different modes are identified by three subscripts m, n, and p, which denote the number of half-wave-length field variations in the azimuthal (ϕ), radial (ρ), and height directions, respectively. The subscript δ is applied when there is less than half-a-wavelength variation in the height-direction. A small number of studies have used DRs in high field MR microscopy [12],[5], as well as one proof-of-principle using a 4 Tesla human scanner [17] using exclusively the $TE_{01\delta}$ mode. The same is true for electron paramagnetic resonance studies, reviewed in Ref. [3]. As shown in Figure 2.1, the $TE_{01\delta}$ mode has a maximum magnetic field component along the major axis of the cylinder (which also corresponds to the location of minimum electric field). However, for MR studies the long axis must be oriented somewhat awkwardly perpendicular to the B_0 field, and it is clearly not possible to operate this mode in quadrature: both of these factors make this mode less than optimal for in vivo imaging experiments. In contrast, two frequency-degenerate orthogonal HEM_{11} modes exist [8] and if the long axis of the cylinder is aligned parallel to B_0 then

quadrature operation is possible. A series of empirical expressions have been derived for the resonance frequencies of the lowest modes of a cylindrical DR [9]. For the HEM_{11} mode this frequency is given by:

$$f_{HEM_{11\delta}} = 2.735 \frac{c\epsilon_r^{-0.436}}{2\pi a}\left[0.543 + 0.589\frac{a}{h} - 0.05\left(\frac{a}{h}\right)^2\right] \tag{2.1}$$

where c is the speed of light, ϵ_r the relative permittivity, a the radius and h the height of the resonator. Although small MR resonators made from high permittivity, low loss materials have been constructed [12],[5], these have required sophisticated fabrication processing involving high pressure compression and controlled sintering conditions, which are very difficult for the larger structures required for in vivo imaging. In contrast, simple deionized water has a high relative permittivity (ϵ_r = 78 at room temperature) and relatively low loss at radio-frequencies (although the loss increases significantly in the microwave range). Application of Eq. 2.1 shows that the dimensions (diameter and length) required for the HEM_{11} mode to resonate at 298.1 MHz (7 Tesla) are of the order of centimetres to tens of centimetres, which lie in the range required for in vivo imaging. For practical applications an annular rather than cylindrical shape must be used, with a clear bore through the centre of the cylinder in order to image the volume of interest. In this article, the properties of such a resonator are investigated in terms of design, efficiency and applicability to in vivo imaging of extremities such as the human wrist. In addition, a new method to detune the resonator is proposed, which would allow integration of receive arrays into the overall design.

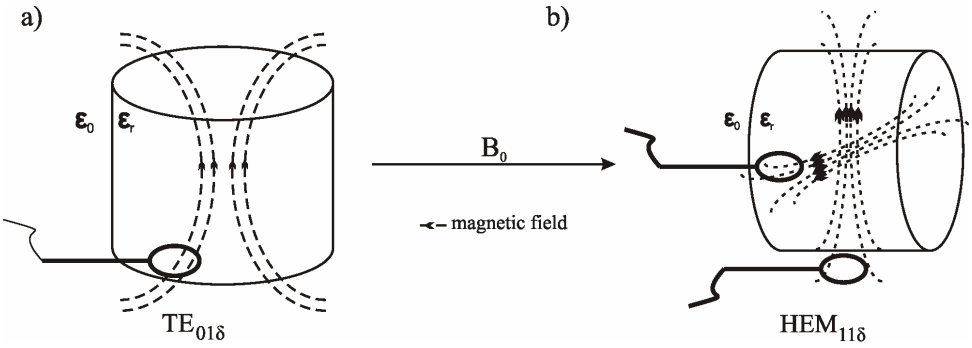

Figure 2.1: Schematic of the magnetic field distributions in the two lowest frequency modes of a cylindrical DR [8]. The $TE_{01\delta}$ mode must be used with the long axis of the cylinder perpendicular to the B0 field, and therefore can only be driven in a linear mode. In contrast, for the $HEM_{11\delta}$ mode the long axis of the cylinder is parallel to B_0 and the two orthogonal modes can be driven in quadrature.

2.2. METHODS

2.2.1. HEM RESONATOR DESIGN

An outer diameter of 140 mm was chosen for the HEM resonator. Based upon Eq.2.1 the HEM_{11} modes resonate at a frequency of 298.1 MHz for a water column height of 72.5 mm. Resonant modes of the water cylinder were detected experimentally using S_{11} measurements from a non-resonant, balanced pick-up loop (diameter 2 cm) on a network analyzer (EN5061, Agilent Technologies, Santa Clara). The $HEM_{11\delta}$ mode was detected using this pick-up loop placed at the side of the resonator: the measured height of the water was 73 mm. The annular HEM_{11} mode resonator was made from two concentric polymethylmethacrylate tubes (Vink Kunststoffen, The Netherlands) creating a cavity of 140 mm outer and 100 mm inner diameters. The height (15.2 cm) of the annulus was obtained empirically on the workbench by filling with distilled water until the HEM_{11} mode was at 298.1 MHz (with a volunteer's wrist in the central bore of the annulus). Polymethylmethacrylate annular rings were constructed and glued to make a closed annulus: filling ports were drilled into the end plates and sealed with a plastic screw and hot glue.

Two inductively coupled impedance matching networks were placed at the centre of the long axis of the resonator at a distance of 3 cm from the outside surface of the resonator, 90 degrees apart from each other. These consisted of 5 cm square coils etched on FR4 PC board, and segmented with three fixed capacitors (American Technical Ceramics, Huntington Station, NY) and two 1–30 pF variable capacitors (Voltronics, Salisbury, MD) for fine tuning. The topology of the coupling loops as well as the impedance matching network is shown in Figure 2.2. The coupling loops were tuned to provide critical coupling to the HEM resonator with a 50 Ohm impedance match. The coil was interfaced to the scanner by using 40 cm long double-shielded 50 Ohm coaxial cables (K02252, Huber & Suhner, Switzerland).

The HEM resonator was matched and tuned when loaded with a human wrist and achieved a S_{11} of –20 dB or better. For different loading conditions (i.e., wrists of different volunteers) the tuning of the HEM resonator itself was not changed, with only slight adjustments to the variable capacitor of the impedance matching circuit required to re-establish critical coupling. A photograph of the HEM coil is shown in Figure 2.2.

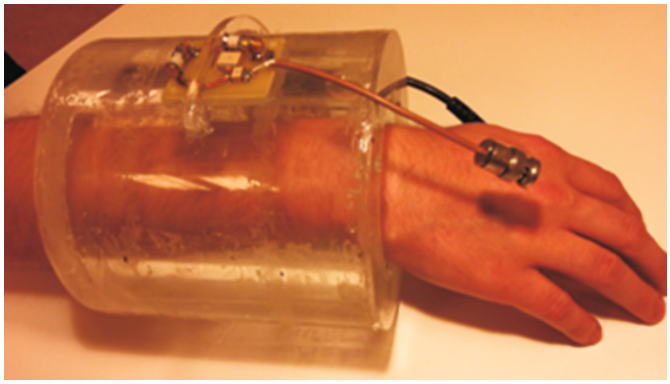

a)

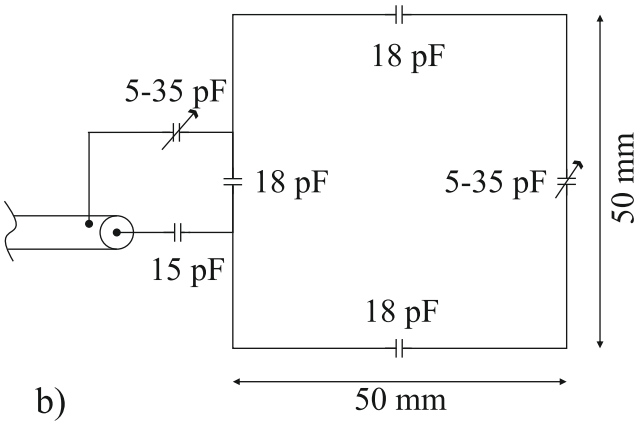

b)

Figure 2.2: a) Photograph of the water-based HEM resonator with quadrature inductive feeds. b) Topology of the coupling loops and the impedance matching network.

2.2.2. DETUNING THE HEM RESONATOR

In order to be able to use the HEM resonator with a receive array it must be electronically detunable. Electrical detuning of a DR by mounting a conducting ring on top of the resonator has been suggested in [7]. However, this only produced a very small change (~75 kHz) for the particular configuration used here.

An alternative detuning mechanism was therefore developed. It was observed that a wire bent into a half circle with legs perpendicular to the half circle shifts the frequency of one of the HEM modes by several tens of MHz if the legs are submersed into the dielectric media while having the half-circle submersed in the medium. If the half-circle is not submerged but positioned slightly above the medium (see Fig. 2.3) then the shift is ~8 MHz. In either case the orthogonal mode is not affected. Rotating the detuning structure by 90 degrees produces the corresponding effect on the orthogonal mode. If a gap (open circuit) is introduced into the centre of the half-circle then the mode structure is not affected, suggesting that introduction of a positive intrinsic negative (PIN)-diode can be used to convert the mechanical structure into an electronically controlled detuning mechanism.

The final detuning device was constructed from a half circle etched out of FR4 (Bungard, Germany) with a diameter of half of the annulus wall width and a track width of 5 mm. In the center of the half circle, a PIN-diode (MA4P7441F-1091, Macom, Lowell, MA) was placed with two series RF chokes of 2600 nH, and 1000 pF blocking capacitors either side. Two stiff copper wires (1.6 mm diameter, length 5 cm) were via-mounted and soldered to the half circle. The wires were then submerged into the HEM resonator through holes parallel to the z-axis of the resonator. The topology of the device is given in Figure 2.3. Detuning of the impedance matching loops was performed using a conventional approach using PIN-diode switching: the topology of this circuit is given in Figure 2.3a.

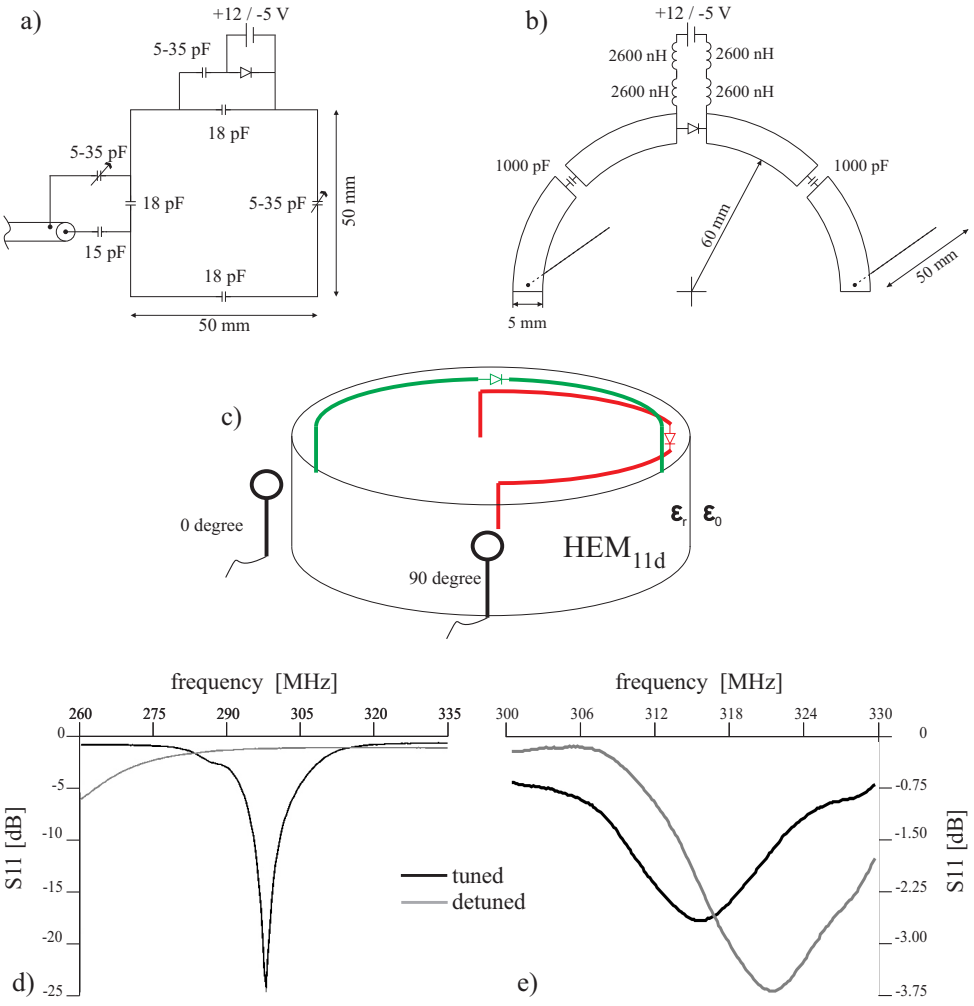

Figure 2.3: a) Topology of the detune-able coupling loops with PIN-diodes. b) Topology of the detuning wire device. c) Schematic of the placement of the detuning devices with respect to the feeding loops. d) S_{11} measurement of the HEM resonator with the coupling loops "tuned" (black line) and "detuned" (gray line). e) S_{11} measurement of the HEM resonator alone (using a nontuned pick-up loop) in the tuned (diodes nonconducting, black line) and detuned (diodes conducting, gray line) cases. Smaller spurious "dips" are due to the pick-up coil itself.

2.2.3. BIRDCAGE COIL

For sensitivity comparisons a quadrature birdcage coil was constructed from the same concentric polymethylmethacrylate tubes (for the RF shield and coil), thus having the same absolute dimensions (outer and inner diameter as well as length) as the HEM resonator. An eight-rung high pass design was used. The rungs and end-rings were constructed from 13 mm wide copper strips (3M, Minneapolis). The end-ring capacitors were 2.1 pF fixed values (American Technical Ceramics, Huntington Station, NY). The two quadrature modes were excited by identical inductive matching networks as those used for the HEM resonator. Fine tuning of the resonance frequency for different loads was performed with additional 1–30 pF variable capacitors in the end rings of the birdcage positioned at 180 degrees to the feed points. The shield was made out of a thin (10 mm) copper sheet wrapped around the outer polymethylmethacrylate cylinder.

2.2.4. COIL CHARACTERIZATION

Two phantoms were used to characterize both coils on the network analyzer: the first phantom consisted of a plastic bottle of 80 mm diameter and a length of 200 mm (1 L volume) filled with mineral oil (ϵ_r 4). The second identically sized phantom was made from 1 L of glycerol solution (Sigma-Aldrich, Germany) with 100 mM NaCl to mimic the relative permittivity (ϵ_r50) and conductivity (σ 0.77 S/m) of human muscle tissue at 298 MHz.

2.2.5. ELECTROMAGNETIC SIMULATIONS

Electromagnetic simulations of the magnetic field distributions for both the cylindrical and annular HEM resonators were performed using a finite difference time-domain (FDTD) solver (XFDTD, Remcom, State College, PA). A single frequency Gaussian excitation pulse was applied at 298.1 MHz, with 30 cycles to ensure steady-state conditions and reached a convergence of –45 dB. The RF shield of the magnet bore was modelled as a thin copper cylinder. A mesh size of 1 by 1 by 1 mm was used for all simulations, as well exact submeshing for all structures smaller than the mesh size. The boundary conditions were chosen as perfectly matched layers with a 30 cell padding around the structure to avoid reflections. As the structure is highly resonant the resonance condition of the unloaded DR was verified by an eigenmode solver simulation (CST, Darmstadt, Germany). Computational time on a 4-core PC was approximately 40 min for the FDTD simulations and 1–2 min for the eigenmode solver. For the evaluation of the local specific absorption

rate (SAR) (10 g average) both coils in the simulation were loaded with a human muscle phantom (relative permittivity 58.2 and conductivity 0.77 S/m) to simulate SAR. Radiation loss in the unshielded HEM was compared to both an unshielded and shielded birdcage.

2.2.6. MRI EXPERIMENTS

All imaging and B_1^+ mapping experiments were conducted on a 7T whole body human MRI scanner (Philips Achieva, Best, The Netherlands). B_1^+1 maps in the oil phantom were produced using the method of Yarnykh et al. [18]. A three-dimensional gradient echo sequence was used with the following parameters: field-of-view (FOV) 160 by 160 by 160 mm^3, voxel resolution 2.5 by 2.5 by 2.5 mm^3, pulse repetition time (TR_1)/TR_2 30/150 ms, echo time 1.5 ms, nominal 45° tip angle at the centre of the phantom. The coil sensitivity was calculated as the B_1^+ per square root Watt of input power, with the power estimated from the measured output power of the RF amplifier taking into account measured power loss in the cables from the amplifier to the coil. Phantom experiments to characterize the linear, quadrature and anti quadrature modes of the HEM resonator used multi-slice gradient echo and spin echo sequences. Gradient echo parameters: FOV 200 by 200 by 52 mm, spatial resolution 1 by 1 by 3 mm, 16 slices, TR 82 ms, echo time 2.6 ms, tip angle 20°. Spin echo parameters: FOV 200 by 200 by 52 mm, spatial resolution 2 by 2 by 3 mm, TR 710 ms, echo time 10 ms. Images of the wrist of a healthy human volunteer were acquired using both gradient echo and spin echo sequences. Gradient echo: multi slice sequence, TR 249.5 ms, echo time 3.9 ms, tip angle 20°, data matrix 320 by 320, slice thickness 2 mm, in-plane resolution 0.5 by 0.5 mm. Spin echo: multi-slice turbo spin echo sequence, TR 8419 ms, echo time 35 ms, turbo spin echo factor 8, data matrix 332 by 216, slice thickness 2 mm, in-plane resolution 0.5 by 0.5 mm, 1 signal average, total imaging time 7 min 50 s. The study adhered to the LUMC Institutional Review Board guidelines and informed consent was obtained prior to the study.

2.3. RESULTS

2.3.1. COIL CHARACTERIZATION

NETWORK analyser measurements gave an S_{11} value for each channel of both the birdcage and HEM resonator less than –20 dB in the loaded (glycerol phantom, human wrist) and unloaded (oil phantom) cases. Isolation between the quadrature channels was also greater than 20 dB in both unloaded and loaded situations.
The performance of the detuning device was then evaluated on the bench. When the PIN-diode in the coupling loop was switched the resonance of the coupling loops was lowered about 50 MHz as shown in Figure 2.4d. The detuning of the HEM mode itself by switching the PIN- diode in the wire detuning device was about 50 MHz with the wires immersed in the water (Fig. 2.4e), with a smaller ~10 MHz shift if only the wire legs were immersed.

2.3.2. SIMULATION RESULTS

From Eq. 2.1 a water cylinder of outer diameter 140 mm has HEM_{11} resonances at 298.1 MHz at a height of 72.5 mm. Figure 2.4 shows the simulated magnetic field produced, with a small excitation loop coil placed at the side of the cylinder (for clarity only one linear mode is shown). The expected HEM_{11} mode is shown, with the magnetic field perpendicular to B_0. If the annular coil with the oil phantom in place is simulated, Figure 2.4b, the basic magnetic field distribution of the HEM_{11} mode is maintained, although the magnitude is reduced. As shown in Figure 2.4c, simulating the human wrist as a cylinder of appropriate dielectric and conductivity values (with a realistic diameter less than the inner diameter of the resonator) increases the magnitude of the magnetic field compared to the case with oil, with high homogeneity restored in the transverse plane.
The simulations showed that the local maximum for the 10 g average SAR for the HEM resonator was ~15% higher compared to the birdcage resonator for the same net system input power (1 W) and normalized to 1 W dissipated power. The radiation losses were ~15% for the (unshielded) HEM resonator, 28% for the unshielded birdcage, and 12 for the shielded birdcage.

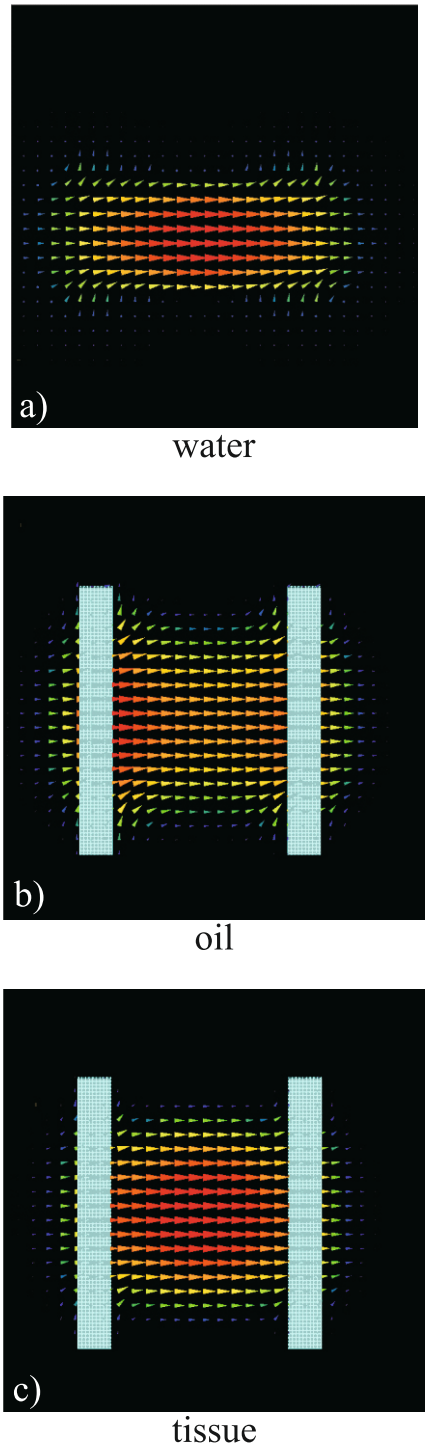

Figure 2.4: Electromagnetic simulations of the magnitude (color) and phase (direction of arrow) of the magnetic field for different configurations of the HEM resonator. a) Cylinder of water, diameter 140 mm, height 72.5 mm. b) Annulus of water, outer diameter 140 mm, inner diameter 100 mm, height 152 mm with an inner cylinder of oil ($\epsilon_r = 4$, outlined by the dotted line) with outer diameter 98 mm. c) Annulus of water, outer diameter 140 mm, inner diameter 100 mm, height 152 mm with an inner cylinder of tissue ($\epsilon_r = 50$, $\sigma = 0.77$ S/m, outlined by the dotted line) with outer diameter 80 mm to simulate the human wrist.

2.3.3. PHANTOM EXPERIMENTS

Figure 2.5 shows axial and coronal images acquired from the oil phantom with the HEM resonator. Both the gradient echo and spin echo images acquired in quadrature mode show a homogeneous signal distribution within the sample. The two separate linear modes show reduced (and mirrored) homogeneity compared to the quadrature mode, as expected. The antiquadrature mode shows very efficient "signal destruction" in the sample, indicating that the two modes are indeed circular polarized.

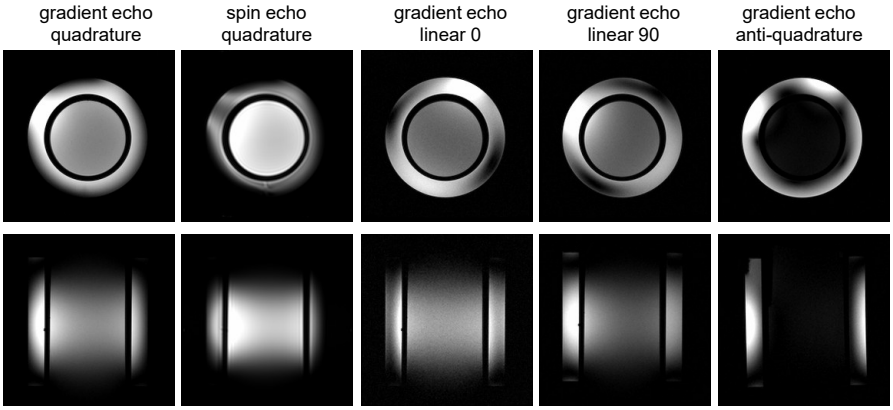

Figure 2.5: Images of an oil phantom placed symmetrically within the HEM resonator.

Experimentally acquired B_1^+ maps are shown in Figure , showing homogeneous fields in both the transverse and longitudinal directions. The magnitude of the B_1^+ field in the oil phantom is very similar to that in the water of the resonator itself. Of course this is also true for the birdcage coil, in which a large amount of energy is stored between the RF coil and the shield (although this is not possible to visualize experimentally). As a measure of the transmit field efficiency, the B_1^+ field at the centre of the phantom was determined to be 2.2 $\mu T/\sqrt{W}$ of power delivered to the coil, i.e., taking into account losses between the

RF amplifier and coil interface.

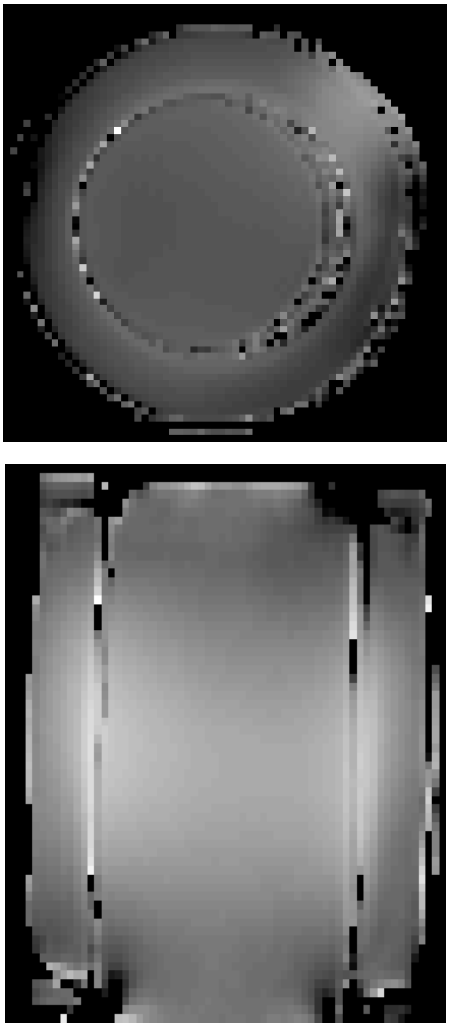

Figure 2.6: Experimentally measured B_1^+ maps in two orthogonal axes from the HEM resonator. The sensitivity at the centre of the coil is 2.2 $\mu T/\sqrt{W}$

The B_1^+ field at the centre of the phantom for the birdcage was slightly higher, with a value of 2.3 $\mu T/\sqrt{W}$. The longitudinal coverage of the HEM and birdcage coils is compared in Figure 2.7. The birdcage is seen to have a slightly broader region of homogeneity

in the centre of the FOV for the particular length-to-diameter ratio used in this article.

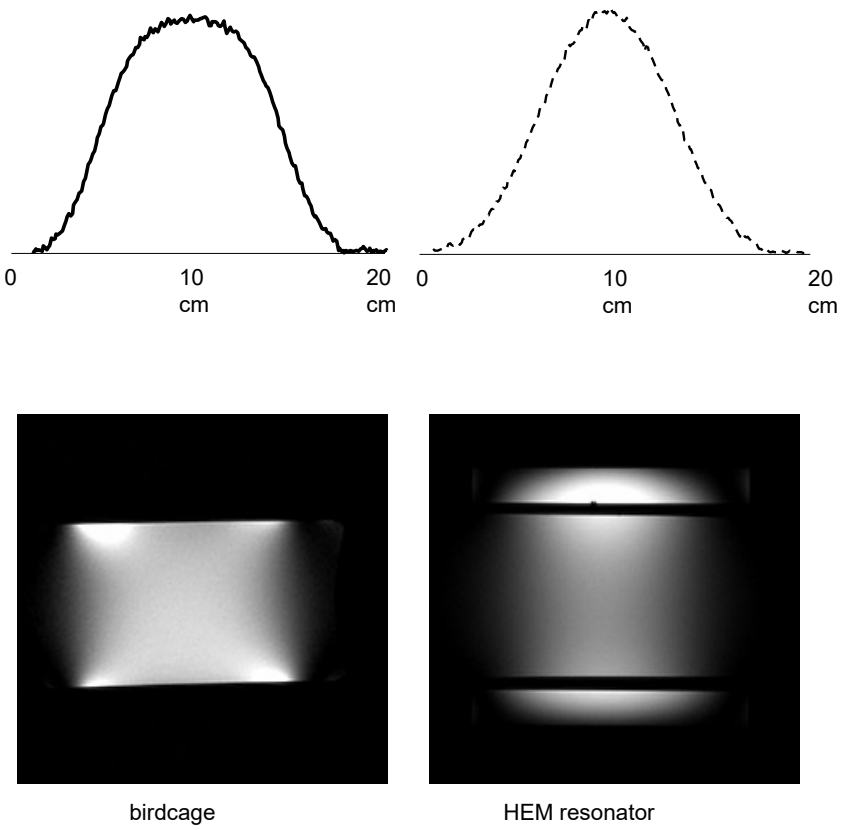

Figure 2.7: Two gradient echo images showing the longitudinal coverage of the birdcage coil (left) and HEM resonator (right).

2.3.4. IN VIVO RESULTS

Figure 2.8 shows coronal gradient echo and spin echo images from the wrist of a healthy volunteer, positioned as shown in Figure 2.2. Good visualization of the cartilage and trabecular bone is evident, as is the reasonable homogeneity in both transverse and axial dimension. No attempt was made to rigorously optimize data acquisition parameters.

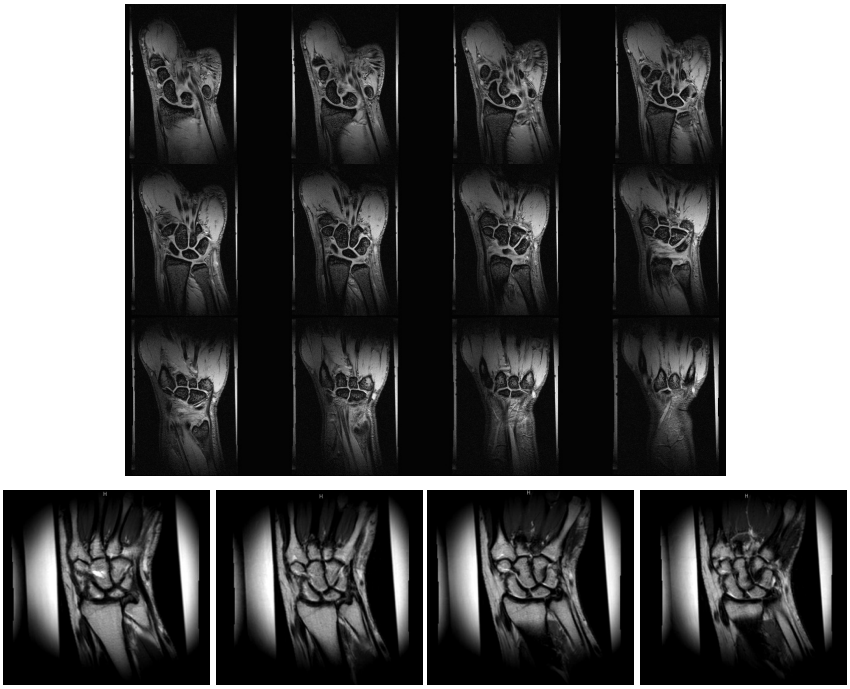

Figure 2.8: (top) Series of coronal multislice gradient echo images acquired in the human wrist using the HEM resonator. (bottom) Spin-echo images acquired using a turbo spin echo sequence

2.4. DISCUSSION

THE results presented here show that the HEM_{11} mode of a water-based DR is a promising new design for high frequency MRI. The design and construction are extremely simple, and the performance has been shown to be essentially identical to that of an equivalently-sized birdcage coil. It should be noted, however, that this sensitivity comparison is extremely conservative in the sense that the dimensions of the resonators are heavily weighted towards the optimum length-to-diameter ratio for the birdcage. Given the intrinsic nature of the HEM mode one can anticipate that a high degree of B_1 uniformity would be maintained for much smaller length-to-diameter ratios, for which the performance of the birdcage resonator degrades significantly. Considering the modes shown in Ref. [16], ratios of as low as 1:4 still produce relatively homogeneous fields, whereas the birdcage would be unusable at such dimensions. In order for the DR to be as flexible as conventional coil designs, it must ideally be possible to integrate with a receive array, which requires that the resonator be detunable. Although one can add a parallel LC tank circuit to the impedance matching network, this does not alter the fact that there is still a tuned resonator. The method investigated involved a simple geometrical arrangement of two wires which shifts the frequency of the HEM mode by tens of MHz if immersed in the water, and ~10 MHz if placed outside the plastic end of the resonator.

One of the potential limitations of the resonator design is that the operating frequency is dictated by only two parameters, namely the size of the resonator and the permittivity of the material used for construction. As such it lacks the inherent flexibility of lumped-element designs in which the use of variable capacitors decouples, to some degree, the resonant frequency from the size of the resonator. Nevertheless, using miscible liquids, it is relatively easy to fine-tune the permittivity of the DR to achieve the desired resonant mode for a particular size of resonator. For a much larger coil, a lower value of permittivity would be required. For example, liquids such as acetone (relative permittivity 20), alcohols (relative permittivities 20–40), and water can be mixed according to simple rules [13] to achieve a given permittivity. While the current demonstration uses water, a practical realization could easily incorporate deuterium oxide to remove the unwanted signal from the coil itself, as also suggested by Wen et al. [17]. Use of high permittivity low loss solid materials would enable smaller resonators to be designed.

The design of DRs is easily extended to higher frequencies and larger coils. Optimization of the exact dimensions/shape/relative permittivity in terms of signal-to-noise and sensitivity is an area in which little research has so far been performed. This general class

of resonators fits into the genre of "leaky waveguides" [6], and share similarities with another coil design suggested for imaging the carotid artery [10]. Given the interplay between resonant conditions and waveguide leakiness it is certainly possible that other geometries can be found which are even more efficient than the one presented here. Mechanistically, it is also possible that "surface waves" [2], which are very familiar from the optical literature, may play a role in the distribution of the RF field throughout the resonator and also, therefore, within the sample.

One area in which this type of resonator may play a role in the future is in the design of PET/MR or SPECT/MR animal and human systems. Although the resonator was fed inductively in the centre of the long-axis in this work, coupling can equally well be performed at the end of the resonator using micro-strips, wave guides, coaxial lines, or dipoles. In terms of the imaging field of view (FOV) the resonator would be completely symmetric, and water results in low attenuation of both PET and SPECT radiation. It is well known that the differential attenuation of spaced conductor structures associated with all conventional RF coil designs cause significant image artefacts in reconstructed nuclear medicine images, and this effect would be eliminated using these types of DRAs.

REFERENCES

[1] G. Adriany, V. de Moortele, F. Wiesinger, S. Moeller, J. P. Strupp, P. Andersen, C. Snyder, X. Zhang, W. Chen, K. P. Pruessmann, et al. Transmit and receive transmission line arrays for 7 tesla parallel imaging. *Magnetic resonance in medicine*, 53(2):434–445, 2005.

[2] V. Agranovich and D. Mills. Surface polaritons: electromagnetic waves at surfaces and interfaces. *Journal of the Optical Society of America B Optical Physics*, 1:410, 1984.

[3] G. Annino, M. Cassettari, I. Longo, M. Martinelli, P. Van Bentum, and E. Van der Horst. A novel probe head for high-field, high-frequency electron paramagnetic resonance. *Review of scientific instruments*, 70(3):1787–1793, 1999.

[4] S. A. Aussenhofer and A. G. Webb. Design and evaluation of a detunable water-based quadrature hem11 mode dielectric resonator as a new type of volume coil for high field mri. *Magnetic Resonance in Medicine*, 68(4):1325–1331, 2012.

[5] K. Haines, T. Neuberger, M. Lanagan, E. Semouchkina, and A. Webb. High q calcium titanate cylindrical dielectric resonators for magnetic resonance microimaging. *Journal of Magnetic Resonance*, 200(2):349–353, 2009.

[6] J. Hu and C. R. Menyuk. Understanding leaky modes: slab waveguide revisited. *Advances in Optics and Photonics*, 1(1):58–106, 2009.

[7] D. Kajfez. *Dielectric Resonators*. INSTITUTION ENGINEERING & TECH, 1998.

[8] D. Kajfez, A. W. Glisson, and J. James. Computed modal field distributions for isolated dielectric resonators. *IEEE transactions on Microwave Theory and Techniques*, 32(12):1609–1616, 1984.

[9] A. Kishk, A. Glisson, and G. Junker. Bandwidth enhancement for split cylindrical dielectric resonator antennas. *Progress In Electromagnetics Research*, 33:97–118, 2001.

[10] W. Koning, J. Bluemink, E. Langenhuizen, A. Raaijmakers, A. Andreychenko, C. den Berg, P. Luijten, J. Zwanenburg, and D. Klomp. High-resolution mri of the carotid arteries using a leaky waveguide transmitter and a high-density receive array at 7 t. *Magnetic Resonance in Medicine*, 69(4):1186–1193, 2013.

[11] G. J. Metzger, C. Snyder, C. Akgun, T. Vaughan, K. Ugurbil, V. de Moortele, et al. Local b1+ shimming for prostate imaging with transceiver arrays at 7t based on subject-dependent transmit phase measurements. *Magnetic Resonance in Medicine*, 59(2):396–409, 2008.

[12] T. Neuberger, V. Tyagi, E. Semouchkina, M. Lanagan, A. Baker, K. Haines, and A. Webb. Design of a ceramic dielectric resonator for nmr microimaging at 14.1 tesla. *Concepts in Magnetic Resonance Part B: Magnetic Resonance Engineering*, 33(2):109–114, 2008.

[13] A. Sihvola. Mixing rules with complex dielectric coefficients. *Subsurface Sensing Technologies and Applications*, 1(4):393–415, 2000.

[14] J. Vaughan, G. Adriany, C. Snyder, J. Tian, T. Thiel, L. Bolinger, H. Liu, L. DelaBarre, and K. Ugurbil. Efficient high-frequency body coil for high-field mri. *Magnetic resonance in medicine*, 52(4):851–859, 2004.

[15] J. T. Vaughan, H. P. Hetherington, J. O. Otu, J. W. Pan, and G. M. Pohost. High frequency volume coils for clinical nmr imaging and spectroscopy. *Magnetic Resonance in Medicine*, 32(2):206–218, 1994.

[16] A. Webb. Visualization and characterization of pure and coupled modes in water-based dielectric resonators on a human 7t scanner. *Journal of Magnetic Resonance*, 216:107–113, 2012.

[17] H. Wen, F. A. Jaffer, T. J. Denison, S. Duewell, A. S. Chesnick, and R. S. Balaban. The evaluation of dielectric resonators containing h 2 o or d 2 o as rf coils for high-field mr imaging and spectroscopy. *Journal of Magnetic Resonance, Series B*, 110(2):117–123, 1996.

[18] V. L. Yarnykh. Actual flip-angle imaging in the pulsed steady state: a method for rapid three-dimensional mapping of the transmitted radiofrequency field. *Magnetic resonance in Medicine*, 57(1):192–200, 2007.